Generation of tunable few optical-cycle pulses by visible-to-infrared frequency conversion

J. Darginavičius · G. Tamošauskas · A. Piskarskas · G. Valiulis · A. Dubietis

Abstract We demonstrate a simple method for infrared few optical-cycle pulse generation, which is based on collinear visible-to-infrared frequency conversion and involves difference-frequency generation and subsequent two-step optical parametric amplification. The numerical simulations and experiments using BBO crystals show an efficient frequency down conversion of visible ∼20 fs pulses from a commercial blue-pumped noncollinear optical parametric amplifier yielding 1.2–2.4 μm tunable sub-100 μJ pulses with duration of 3 to 5 optical-cycles. The proposed method could be readily extended to generate few optical-cycle pulses in the mid-infrared spectral range (up to 5.5 μm) using, e.g., $LiIO_3$ and $LiNbO_3$ crystals, as demonstrated by the numerical simulations. In these crystals, even shorter, two-optical-cycle mid-infrared pulses could be obtained at particular wavelengths where group velocity matching between the signal and idler waves is achieved.

1 Introduction

Thanks to unique properties, such as high gain and broad amplification bandwidth that are achievable over wide spectral range, optical parametric amplification became the most advanced technique to extend the tunability range of the ultrashort pulse lasers. Modern optical parametric amplifiers deliver powerful femtosecond pulses tunable across the visible and near infrared (IR) [1–5]. At present, there is a growing demand for energetic, few-optical cycle pulses in the near and mid-IR in connection with ultrafast spectroscopy [6–8] and rapidly evolving discipline of strong field physics and attosecond science [9]. In the pursuit of this goal, various approaches and strategies enabling efficient generation of few optical-cycle pulses in the IR spectral range have been proposed. A straightforward route to generate few optical-cycle pulses in the IR is to pump an optical parametric amplifier (OPA) with extremely short pulses, obtained, e.g., by employing hollow-fiber compression technique [10], which however imposes severe limitations on the available pump energy. Another approach considers the use of broadband phase matching that is readily achievable in a collinear interaction geometry at the degeneracy, at the cost of wavelength tunability [11]. More flexible methods utilize the noncollinear optical parametric amplification technique in nonlinear crystals, which provide suitable group velocity relations in the IR; see [5] for a review and recent developments in the field. The noncollinear infrared optical parametric amplifiers commonly employ the infrared part of the supercontinuum as a seed signal, whose low spectral energy density imposes certain practical difficulties, such as high level of the amplified parametric superfluorescence. Frequency down-shifting (i.e., difference-frequency generation, DFG) of already preformed seed pulse proves to be more energetically efficient and is demonstrated in a number of experimental configurations, which use various transparent media with quadratic and cubic nonlinearity [12–15]. High power and high repetition rate OPCPA technique-based systems, which combine either optical parametric amplification and/or difference frequency generation with nonlinear propagation (hollow-fiber or filamentation) techniques at present yield high energy (tens-of-mJ), high peak-power (sub-100-GW) few-optical cycle pulses whose wavelength is now shifted into the mid-IR [16–20].

J. Darginavičius (✉) · G. Tamošauskas · A. Piskarskas · G. Valiulis · A. Dubietis
Department of Quantum Electronics, Vilnius University, Saulėtekio 9 bldg. 3, 10222 Vilnius, Lithuania
e-mail: Julius.Darginavicius@ff.stud.vu.lt

More recently, several methods for few optical-cycle IR pulse generation based on visible-to-infrared frequency conversion in very compact setups were demonstrated [21–23]. In this paper, we propose a simple and efficient method for few optical-cycle infrared pulse generation, which is based on collinear difference-frequency conversion and two-stage optical parametric amplification of unchirped femtosecond pulses. The experimental demonstration employs a fully commercial Ti:sapphire laser and its second-harmonic pumped noncollinear optical parametric amplifier system, whose tuning range is extended into the IR using a setup for visible to infrared frequency conversion based on BBO crystals providing 1.2–2.4 μm tunable pulses with 3 to 5 optical-cycle duration and sub-100 μJ energy. The achieved tuning range could be readily extended by using nonlinear crystals with wider IR transparency range maintaining few optical-cycle pulse duration, as revealed by the numerical simulations.

2 The general idea

The general idea of the proposed method is schematically depicted in Fig. 1. Tunable few optical-cycle IR pulses are obtained by means of two-step collinear second-order parametric interactions: difference-frequency generation and subsequent optical parametric amplification of the difference-frequency signal. In contrast to widely used schemes that involve optical parametric amplification of the IR part of the supercontinuum spectrum, the proposed scheme benefits from using already well-established ultra-short visible light pulses, which are of excellent spatial and temporal quality and high energy.

The first step involves frequency down-conversion of the ultrashort visible pulses via type I phase-matched difference-frequency generation. Here, by mixing of the e-polarized visible pulse at ω_{vis} from a blue-pumped non-collinear optical parametric amplifier (NOPA) and the o-polarized fundamental frequency pulse at ω_p from an amplified Ti:sapphire laser system, the o-polarized few optical-cycle pulse at $\omega_{MIR} = \omega_{vis} - \omega_p$ in the mid-IR (MIR) is produced. In the second step, the o-polarized difference-frequency pulse at ω_{MIR} serves as a seed signal in a
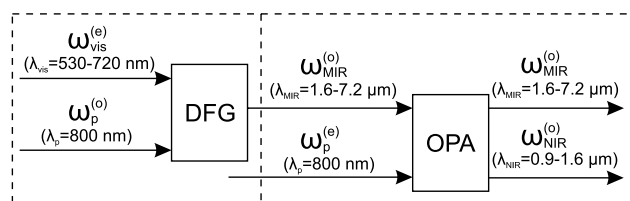
collinear type I phase-matched OPA pumped by the e-polarized fundamental frequency pulse at ω_p from an amplified Ti:sapphire laser system. Alongside amplification of the seed, the OPA produces the o-polarized near-IR (NIR) idler wave at ω_{NIR}. Note that the OPA is seeded with a longer wavelength pulse, which is then called a signal pulse throughout the text. Specifically, in this configuration, by tuning wavelength of the visible pulse in the $\lambda_{vis} = 530–720$ nm range, which is defined by the blue-pumped NOPA operational characteristics, the tunable MIR and NIR pulses that cover wavelength range of $\lambda_{MIR} = 1.6–7.2$ μm and $\lambda_{NIR} = 0.9–1.6$ μm, respectively, could be generated; see Fig. 1. The actual tuning range, however, will depend on the IR absorption properties of the particular nonlinear crystal used. For instance, using the BBO crystal, the tuning range is limited to wavelengths shorter than 3 μm, being set by the crystal absorption in the IR. On the other hand, the tuning range could be notably extended by choosing nonlinear crystals, such as, e.g., $LiIO_3$ or $LiNbO_3$, which are transparent up to 6 μm and 5.5 μm, respectively.

3 Visible-to-infrared conversion in BBO crystals

In this section, we present the numerical simulations and experimental demonstration of the proposed method using a setup based on BBO crystals.

3.1 Numerical simulations

As a starting point, we present the results of the numerical simulations, which illustrate the basic performance characteristics of the DFG and OPA stages. The numerical simulations were carried out by solving the three-wave parametric equations in the framework of plane wave approximation with account for group velocity mismatch, group velocity dispersion, and third-order dispersion effects. The relevant parameters of the BBO crystal (nonlinearity, dispersion relation, transparency range, etc.) were taken from [24].

The DFG process was simulated using input Gaussian pulses with FWHM widths of $t_{vis} = 20$ fs and $t_p = 130$ fs, as those used in real experimental settings (see Sect. 3.2 for details). Note that both input pulses are considered to be bandwidth limited, i.e., no temporal stretching and pulse chirping is applied. The most favorable conditions for DFG in terms of acceptance bandwidth and conversion efficiency for wavelengths of interest occur in type I phase matching interaction. The FWHM width of the difference-frequency pulse versus wavelength as computed by numerical integration of coupled-wave equations for three different lengths (0.1, 0.2, and 0.4 mm) of the BBO crystal is depicted in Fig. 2. The total intensity of the input pulses ($I_{vis} + I_p$ and
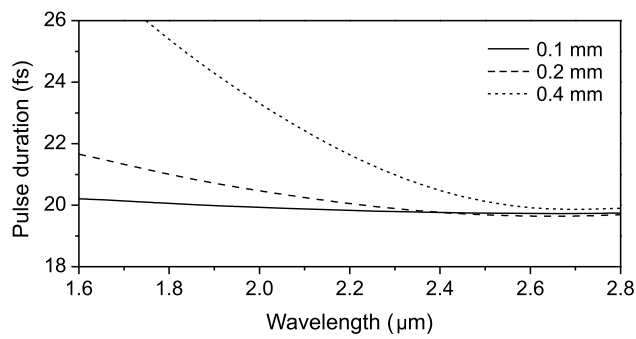

Fig. 1 Schematic presentation of the visible-to-infrared frequency conversion method

Fig. 2 Computed FWHM width of the difference-frequency pulse generated in 0.1 mm (*solid curve*), 0.2 mm (*dashed curve*), and 0.4 mm (*dotted curve*) BBO crystals

Fig. 3 (**a**) Group velocity mismatch between the signal and idler pulses in BBO crystal. (**b**) Computed FWHM pulsewidth as a function of wavelength at the OPA output, which uses 0.5 mm and 1 mm BBO crystals. (**c**) Temporal pulse profiles of the depleted pump (*black*), amplified signal at 2 µm (*blue*) and idler at 1.33 µm (*red*). The *dashed curves* show phases of the signal and idler pulses, respectively

$I_{vis} \approx I_p$) was set at 300, 100, and 50 GW/cm^2, respectively, so as to obtain ~50 % energy depletion of the highest frequency (visible) pulse. Note that in a difference frequency mixing process, the highest frequency wave is depleted, whereas both lower frequency waves are amplified. Under the chosen parameters of interaction, the BBO crystal of 0.2 mm thickness was found to be optimal, as it provided the best compromise between the energy conversion efficiency [$E_{MIR}/(E_{vis} + E_p) = 2.5$ %] and attainable pulse width (the pulse broadening being less than 10 % across the entire tuning range).

Further, we simulate the operation of a difference-frequency pulse-seeded collinear OPA, which was pumped by $t_p = 130$ fs fundamental laser pulse. We investigate parametric amplification in BBO crystals of 0.5 mm and 1 mm thickness by choosing a fixed seed pulse intensity of 1 GW/cm^2 and the pump pulse intensities of 350 GW/cm^2 and 100 GW/cm^2 set for shorter and longer crystals, respectively, so as to obtain 15 % pump-to-infrared conversion efficiency with a gain factor of ~100. Figure 3(a) shows the calculated group-velocity mismatch (GVM), $1/v_s - 1/v_i$, between the signal and idler pulses, which essentially defines the accessible amplification bandwidth. Figure 3(b) summarizes the numerically computed FWHM width of the signal and idler pulses across the entire tuning range. Figure 3(c) shows an example of computed temporal profiles and phases of the interacting pulses ($\lambda_s = 2$ µm, $\lambda_i = 1.33$ µm) at the output of 1-mm-thick BBO crystal. Note how the pump pulse is almost completely depleted in the area where the pulses overlap; the time separation between the signal and idler pulses at the crystal output is markedly reduced due to strong nonlinear interaction. Moreover, the use of unstretched and unchirped seed pulses in the OPA pays-off with regard of achieved pulse width; note that the amplified pulse lengthening is quite small and does not exceed 30 % even at the very edges of the tuning range.
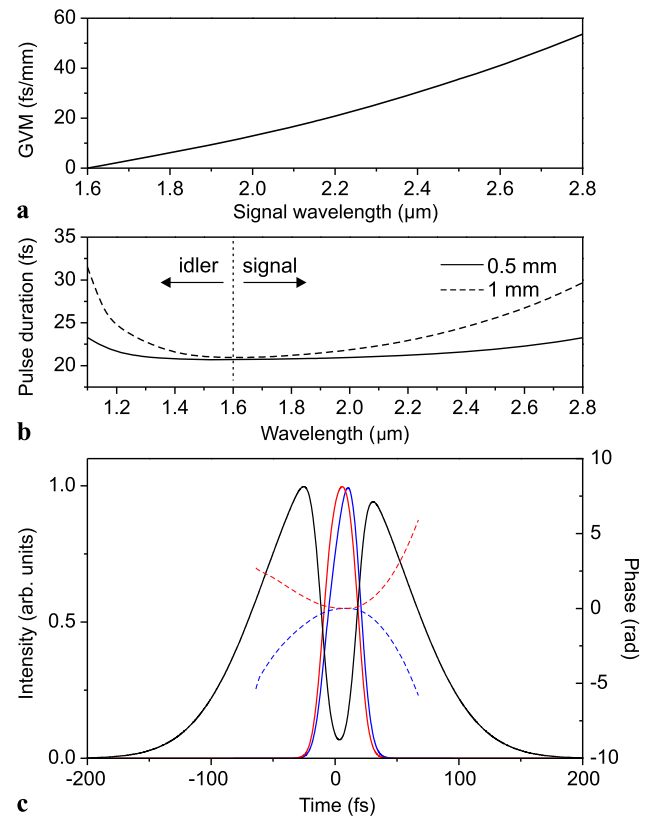
3.2 Experimental results

The validity of the numerical results was verified experimentally. The experimental setup is depicted in Fig. 4. We used a commercial amplified Ti:sapphire laser system (Spitfire-PRO, Newport-Spectra Physics), which delivered 130 fs, ~1.5 mJ pulses with central wavelength of 800 nm. The fundamental laser beam was divided by the beam splitter BS1 into two parts. The first part, with 0.4 mJ energy, was frequency doubled via second-harmonic generation in a 0.5-mm-thick BBO crystal (not shown) and served to pump a supercontinuum-seeded commercial NOPA device (TOPAS-white, Light Conversion Ltd.), which produced 530–720 nm tunable 15–25 fs pulses with energy of ~5 µJ. The second part of the laser beam was divided into three channels (beam splitters BS2 and BS3) with energy of 15 µJ, 150 µJ and 1 mJ that served to pump the difference-frequency generator (DFG), preamplifier (OPA1) and power amplifier (OPA2), respectively.

The difference-frequency generation was performed in a 0.2-mm-thick BBO crystal cut at 29.2° for type I phase matching. The input beams (NOPA output and laser fun-
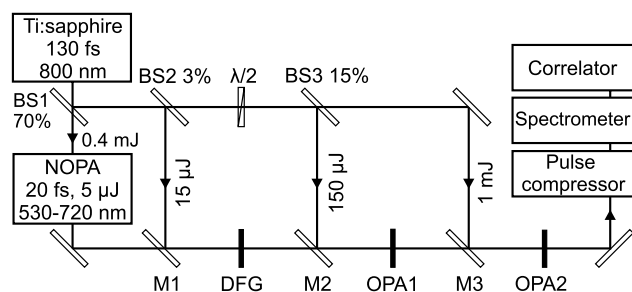
Fig. 4 Experimental setup: *DFG* is the difference frequency generator, *OPA1* is the preamplifier, *OPA2* is the power amplifier, *BS1*, *BS2*, and *BS3* are the beam splitters, $\lambda/2$ is a half-wave plate, *M1* is a dichroic mirror (transparent in the visible and highly reflective at 800 nm), *M2* and *M3* are the dichroic mirrors transparent in IR and highly reflective at 800 nm

Fig. 5 Comparison of the pulse spectra after the difference-frequency generator (*dotted curve*), and at the output of the preamplifier (*dashed curve*) and power amplifier (*solid curve*)

Fig. 6 (**a**) Spectra of the visible, NIR and MIR pulses centered at 575 nm, 1.31 μm, and 2.06 μm, respectively. (**b**) Pulse duration versus wavelength. The *dashed lines* indicate the pulse duration with $N = 3$, 4, and 5 optical-cycles

damental) were arranged in a collinear geometry using a dichroic mirror M1. The beams were focused to a spot size of ~0.5 mm with a spherical $f = +300$ mm lens thus achieving peak intensities of the input pulses of $I_{vis} = 65$ GW/cm^2 and $I_p = 30$ GW/cm^2. Under these experimental conditions, the difference-frequency pulses with 200–400 nJ energy throughout the whole 1.6–2.4 μm range were generated. These further served to seed the OPA, which consisted of preamplifier and power amplifier, both based on type I phase matching BBO crystals. In order to fulfill type I phase matching condition, the polarization of the pump wave was rotated by 90° using a $\lambda/2$ plate placed in front to the beam splitter BS3.

The preamplifier used a 0.5 mm-thick BBO crystal, which was pumped by loosely focused 150 μJ fundamental pulse. The FWHM beam diameter at the crystal input face was 0.45 mm, yielding the pump pulse intensity of 450 GW/cm^2. The pump and seed beams were arranged in a slightly non-collinear geometry (the crossing angle $<1°$) so as to easily separate the signal (1.6–2.4 μm) and idler (1.2–1.6 μm) beams of the same polarization. The preamplifier operated with 10 % energy conversion efficiency, delivering 2–4 μJ signal pulses. Thereafter, these pulses were sent to a power amplifier, which used 1-mm-thick BBO crystal and which was pumped by the rest of the laser energy (1 mJ) in a collimated beam with FWHM diameter of 1.6 mm and intensity of 250 GW/cm^2. The power amplifier delivered a total of 120 μJ energy, which was distributed between the signal and idler waves according to Manley–Rowe relation. For instance, at signal and idler wavelengths of 2.06 μm and 1.31 μm, where pulses were characterized (see below), the measured energy of the signal and idler waves was 45 μJ and 75 μJ, respectively.

The spectral characteristics of the pulse at 2.06 μm at relevant stages of the experiment are depicted in Fig. 5, which compares pulse spectra after the difference-frequency generation, and at the outputs of the preamplifier and power
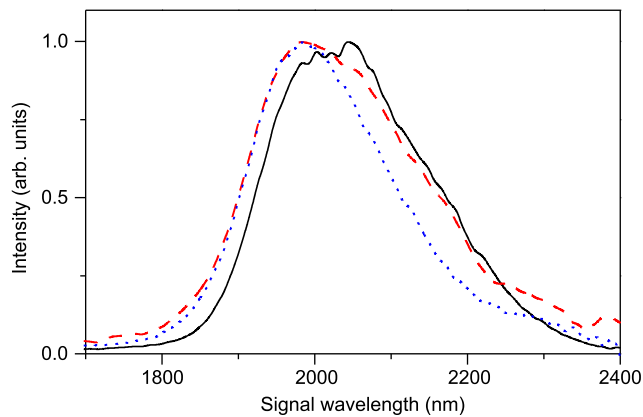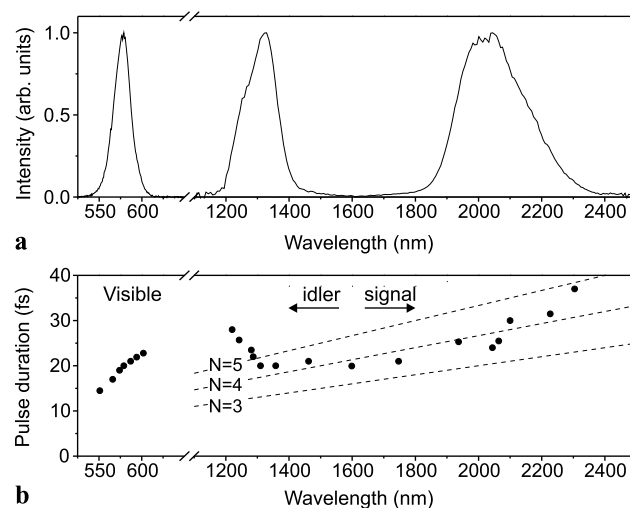
amplifier, as measured using fiber spectrometer (AvaSpec-NIR256-2.5, Avantes). Note that the modifications of the spectral shape imposed by the optical parametric amplification process are very minor: the observed spectral narrowing was estimated to be less than 10 %, in good agreement with the results of numerical simulations. The measured FWHM spectral width at the output of the power amplifier was ~250 nm, that corresponded to 24 fs transform-limited pulse duration.

Figures 6 and 7 summarize the main experimental results. Figure 6(a) shows spectra of the visible pulses at 575 nm and the amplified MIR (signal) and NIR (idler) pulses centered at 2.06 μm and 1.31 μm, respectively. Figure 6(b) shows the temporal characteristics across the whole tuning range by presenting the measured pulse width of the visible pulses at the NOPA output and the estimated pulse width of the
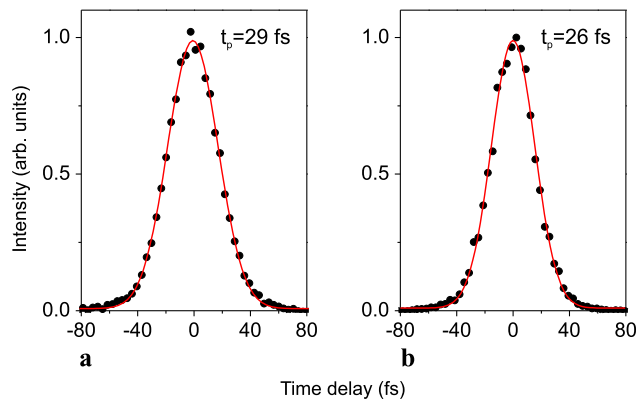
Fig. 7 Autocorrelation traces of compressed pulses: (**a**) signal pulse at 2.06 μm, (**b**) idler pulse at 1.31 μm. Full circles show the experimental data, solid curves show Gaussian fit

signal (MIR) and idler (NIR) waves as derived from spectral measurements and subsequent Fourier transform. The dashed lines indicate the pulse width, which corresponds to $N = 3$, 4, and 5 optical-cycles. The experimental data are in fair agreement with the results of numerical simulations, presented in Fig. 3(b).

Figure 7 shows the autocorrelation traces of compressed signal and idler pulses as measured by a scanning autocorrelator. It has to be mentioned that although we consider parametric amplification of unchirped signal pulse, in fact, in the experiment it became negatively chirped (blue-shifted frequencies at the leading front and red-shifted frequencies at the trailing front) due to anomalous material dispersion introduced by the optical elements of the setup (focusing lenses, dichroic mirrors, and autocorrelator optics) in the 1.6–2.4 μm wavelength range. Indeed, the measured duration of the signal pulse at 2.06 μm directly at the amplifier output was 110 fs. Therefore, the signal pulse was compressed by passing it through a 3-mm-thick ZnSe plate, which possesses normal group velocity dispersion in this spectral range. The autocorrelation trace of compressed signal pulse is plotted in Fig. 7(a), which shows a smooth Gaussian profile. The estimated FWHM pulsewidth of 29 fs (4.2 optical-cycles) thus yielded the time-bandwidth product of $\Delta\tau\Delta\nu \approx 0.51$. Slightly imperfect pulse chirp compensation (measured pulsewidth of 29 fs instead 24 fs as estimated from the spectral width) occurred likely due to higher-order dispersion imposed by ZnSe, as also noted in [20]. The positive chirp of the idler pulse, as attained in the parametric amplification process was compensated in a double-pass TF5 glass prism-pair compressor. The autocorrelation trace of compressed idler pulse at 1.31 μm is shown in Fig. 7(b), which again shows a smooth Gaussian profile. The retrieved FWHM pulsewidth of 26 fs and the time-bandwidth product of $\Delta\tau\Delta\nu \approx 0.46$ attest almost perfect compensation of the idler pulse chirp.
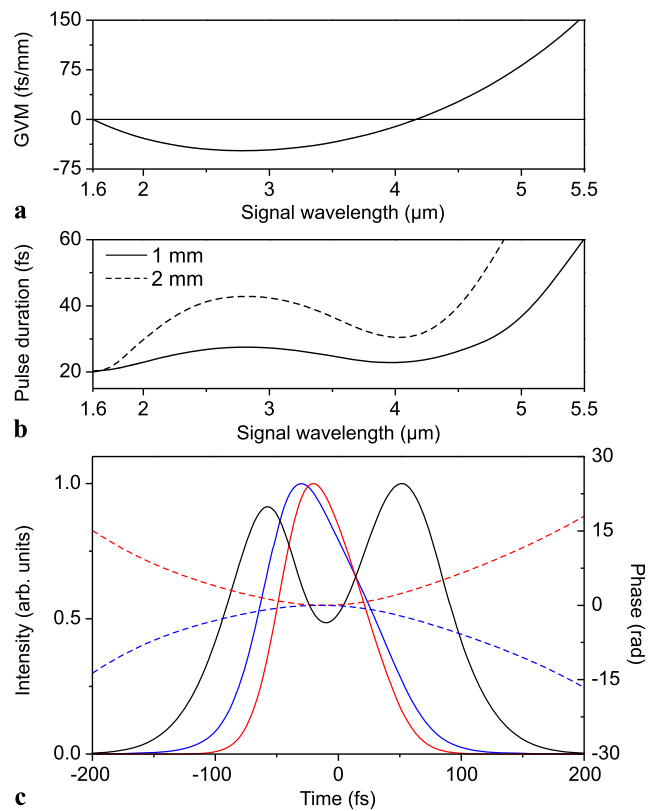

Fig. 8 Performance characteristics of LiIO$_3$ crystal-based OPA. (**a**) GVM between the signal and idler pulses. (**b**) Computed FWHM pulse width versus wavelength in 1 mm (*solid curve*) and 2 mm (*dashed curve*) thick crystals. (**c**) Temporal pulse profiles of the depleted pump (*black*), amplified signal at 4 μm (*blue*) and idler at 1 μm (*red*). The *dashed curves* show phases of the signal and idler pulses, respectively

4 Accessing 3–5.5 μm range

The absorbing properties of the BBO crystal limit the tunability of the IR pulses to wavelengths shorter than 2.6 μm, although the available tuning range of visible pulse wavelengths is suitable to do so, as described in Sect. 2; see also Fig. 1. In what follows, we demonstrate a general possibility to extend the proposed concept for generation of few optical-cycle pulses in the mid-IR. We perform the numerical simulations of difference-frequency pulse-seeded optical parametric amplification in the mid-IR in LiIO$_3$ and LiNbO$_3$ crystals, whose relevant parameters were taken from [24, 25]. Here, we consider an identical situation of the OPA operation as in Sect. 3.1: unchirped ∼20 fs mid-IR seed pulses are amplified in a collinear type I phase matched OPA pumped by 130 fs pulses at 800 nm.

Figure 8 summarizes the results of numerical simulations of parametric amplification in LiIO$_3$ crystal. Figure 8(a) shows the GVM between the signal and idler pulses in the signal wavelength range of 1.6–5.5 μm. Interestingly, apart from the degeneracy, there exists a second group-velocity matching point at 4.2 μm, where conditions for collinear
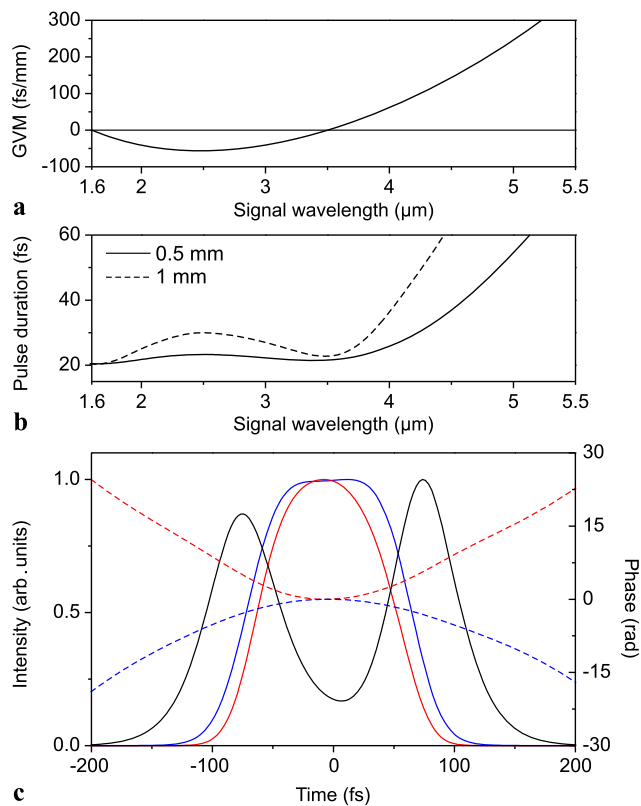
Fig. 9 Performance characteristics of LiNbO$_3$ crystal-based OPA. (**a**) GVM between the signal and idler pulses. (**b**) Computed FWHM pulse width versus wavelength in 0.5 mm (*solid curve*) and 1 mm (dashed curve) thick crystals. (**c**) Temporal pulse profiles of the depleted pump (*black*), amplified signal at 3.5 μm (*blue*) and idler at 1.04 μm (*red*). The *dashed curves* show phases of the signal and idler pulses, respectively

broadband parametric amplification are fulfilled. At longer wavelengths, the group velocity mismatch rapidly increases, thereby limiting the effective tuning range to wavelengths shorter than 5.5 μm due to reduced amplification bandwidth. Figure 8(b) depicts the computed achievable transform-limited FWHM pulse width (after compensation of residual pulse chirp) of the mid-IR signal pulses at the output of the OPA, which uses LiIO$_3$ crystals of 1 mm and 2 mm thickness. Here, optical parametric amplification was simulated using pump pulse intensity of 100 GW/cm^2 that produced gain factors of 5 and 50 in shorter and longer crystals, respectively. Figure 8(c) shows an example of numerically simulated intensity profiles and phases of the interacting pulses in 2-mm-thick LiIO$_3$ crystal at the group-velocity matching point at 4.2 μm.

Figure 9 shows the GVM between the signal and idler pulses in LiNbO$_3$ crystal and basic performance characteristics of LiNbO$_3$ crystal based OPA. Figures 9(a) and (b) show the group velocity mismatch and achievable pulse width, respectively. Here, collinear group velocity matching between the signal and idler pulses occurs at 3.5 μm. Thanks

to larger nonlinear coefficient of LiNbO$_3$, 1-mm-long crystal yields as much a twice gain (~100) than that achieved in twice longer LiIO$_3$ crystal at the same pumping intensity of $I_p = 100$ GW/cm^2. The intensity profiles of the pump, signal, and idler pulses at the output of 1-mm-long LiNbO$_3$ crystal-based OPA are shown in Fig. 9(c).

To summarize the results of numerical simulations, the performance characteristics of LiIO$_3$ and LiNbO$_3$ OPAs are quite similar. However, in choosing a particular value of the pump intensity ($I_p = 100$ GW/cm^2), we did not account for a possible optical damage of the LiIO$_3$ crystal, which is expected to occur at lower intensities than in LiNbO$_3$, since exact optical damage thresholds for these crystals in the femtosecond regime are not precisely known. In both investigated cases, shown in Fig. 8(c) and in Fig. 9(c), the amplified pulses feature some phase modulation, which occurs as a result of group velocity dispersion. Larger group velocity dispersion in LiNbO$_3$ crystal results in somewhat longer pulses with larger chirp at the OPA output. On the other hand, the character of phase modulation in both cases is very regular (quadratic), so it could be readily compensated using an external pulse compressor. Our findings suggest that at particular wavelengths (4.2 μm in LiIO$_3$ and 3.5 μm in LiNbO$_3$) after compensation of residual chirp, pulses with duration shorter than 2 optical-cycles could be obtained.

5 Conclusions

In conclusion, we presented a simple method for visible-to-infrared frequency conversion of unchirped sub-30 fs pulses by collinear difference-frequency generation and subsequent optical parametric amplification, which uses a commercial laser system consisting of an amplified Ti:sapphire laser and second-harmonic pumped noncollinear optical parametric amplifier. As an experimental proof, we demonstrate generation of broadly tunable few optical-cycle pulses using BBO crystals in the wavelength range of 1.2–2.4 μm. After two-stage optical parametric amplification, we obtain sub-100 μJ pulses with 10 % pump-to-infrared conversion efficiency. The validity of the concept is supported by the results of the numerical simulations that also suggest the possibility of tuning range extension further in the mid-IR using the nonlinear crystals with better IR transparency (e.g., LiIO$_3$, LiNbO$_3$). Numerical simulations suggest that thanks to group velocity matching at 3.5 μm in LiNbO$_3$ and at 4.2 μm in LiIO$_3$ crystals, pulses with duration shorter than 2 optical-cycles at these particular wavelengths could be obtained. The proposed method could readily serve for design of compact ultrashort-pulsed IR sources for diverse applications. In particular, pulse energy and tuning range achieved by the developed source would ideally suit for fundamental and applied studies of femtosecond filamentation and re-

lated phenomena in solid state dielectric media under conditions of high order nonlinear absorption and anomalous group velocity dispersion, i.e., in the regime, which is poorly explored up to date [26].

References

1. R. Danielius, A. Piskarskas, A. Stabinis, G.P. Banfi, P. Di Trapani, R. Righini, J. Opt. Soc. Am. B **10**, 2222 (1993)
2. E. Riedle, M. Beutter, S. Lochbrunner, J. Piel, S. Schenkl, S. Spörlein, W. Zinth, Appl. Phys. B **71**, 457 (2000)
3. G. Cerullo, S. De Silvestri, Rev. Sci. Instrum. **74**, 1 (2003)
4. A. Dubietis, R. Butkus, A. Piskarskas, IEEE J. Sel. Top. Quantum Electron. **12**, 163 (2006)
5. D. Brida, C. Manzoni, G. Cirmi, M. Marangoni, S. Bonora, P. Villoresi, S. De Silvestri, G. Cerullo, J. Opt. **12**, 013001 (2010)
6. C. Manzoni, D. Polli, G. Cerullo, Rev. Sci. Instrum. **77**, 023103 (2006)
7. O. Isaienko, E. Bourget, Opt. Express **20**, 547 (2012)
8. D. Brida, C. Manzoni, G. Cirmi, D. Polli, G. Cerullo, IEEE J. Sel. Top. Quantum Electron. **18**, 329 (2012)
9. P.B. Corkum, F. Krausz, Nat. Phys. **4**, 381 (2007)
10. M. Nisoli, S. Stagira, S. De Silvestri, O. Svelto, G. Valiulis, A. Varanavičius, Opt. Lett. **23**, 630 (1998)
11. D. Brida, G. Cirmi, C. Manzoni, S. Bonora, P. Villoresi, S. De Silvestri, G. Cerullo, Opt. Lett. **33**, 741 (2008)
12. C. Manzoni, G. Cerullo, S. De Silvestri, Opt. Lett. **29**, 2668 (2004)
13. T. Fuji, T. Suzuki, Opt. Lett. **32**, 3330 (2007)
14. D. Faccio, A. Grün, P.K. Bates, O. Chalus, J. Biegert, Opt. Lett. **34**, 2918 (2009)
15. E. Rubino, J. Darginavičius, D. Faccio, P. Di Trapani, A. Piskarskas, A. Dubietis, Opt. Lett. **36**, 382 (2011)
16. C. Vozzi, F. Calegari, E. Benedetti, S. Gasilov, G. Sansone, G. Cerullo, M. Nisoli, S. De Silvestri, S. Stagira, Opt. Lett. **32**, 2957 (2007)
17. X. Gu, G. Marcus, Y. Deng, T. Metzger, C. Teisset, N. Ishii, T. Fuji, A. Baltuška, R. Butkus, V. Perval, H. Ishizuki, T. Taira, T. Kobayashi, R. Kienberger, F. Krausz, Opt. Express **17**, 62 (2008)
18. O. Chalus, A. Thai, P.K. Bates, J. Biegert, Opt. Lett. **35**, 3204 (2010)
19. G. Andriukaitis, T. Balčiūnas, S. Ališauskas, A. Pugžlys, A. Baltuška, T. Popmintchev, M.C. Chen, M.M. Murnane, H.C. Kapteyn, Opt. Lett. **36**, 2755 (2011)
20. F. Silva, P.K. Bates, A. Esteban-Martin, M. Ebrahim-Zadeh, J. Biegert, Opt. Lett. **37**, 933 (2012)
21. M. Bradler, C. Homann, E. Riedle, Opt. Lett. **36**, 4212 (2011)
22. J. Darginavičius, E. Rubino, G. Tamošauskas, D. Faccio, G. Valiulis, P. Di Trapani, A. Piskarskas, A. Dubietis, Lith. J. Phys. **51**, 218 (2011)
23. C. Homann, M. Bradler, M. Förster, P. Hommelhoft, E. Riedle, Opt. Lett. 158713 (2012, in press)
24. D.N. Nikogosyan, *Nonlinear Optical Crystals* (Springer, New York, 2005)
25. M.J. Weber, *Handbook of Optical Materials* (CRC Press, Washington, 2003)
26. A. Couairon, A. Mysyrowicz, Phys. Rep. **441**, 47 (2007)